

Copyright is owned by the Author of the thesis. Permission is given for a copy to be downloaded by an individual for the purpose of research and private study only. The thesis may not be reproduced elsewhere without the permission of the Author.

PHYSICOCHEMICAL AND STRUCTURAL STUDIES
ON TWO TRIDENTATE ANTITUMOUR LIGAND SYSTEMS

A thesis presented in partial fulfilment of the requirements for the degree of
Doctor of Philosophy in Chemistry at Massey University.

JOHN DAVID RANFORD

1988

Massey University Library

Thesis Copyright Form

Title of thesis: Physicochemical and Structural
Studies on two Tridentate Antitumour Ligand Systems

(1) (a) I give permission for my thesis to be made available to readers in the Massey University Library under conditions determined by the Librarian.

~~(b)~~ I do not wish my thesis to be made available to readers without my written consent for _____ months.

(2) (a) I agree that my thesis, or a copy, may be sent to another institution under conditions determined by the Librarian.

~~(b)~~ I do not wish my thesis, or a copy, to be sent to another institution without my written consent for _____ months.

(3) (a) I agree that my thesis may be copied for Library use.

~~(b)~~ I do not wish my thesis to be copied for Library use for _____ months.

Signed J.D. Renford
Date 18/10/88

The copyright of this thesis belongs to the author. Readers must sign their name in the space below to show that they recognise this. They are asked to add their permanent address.

NAME AND ADDRESS

27 Epsom Road
Palmerston North

DATE

18/10/88

DEDICATION

To all the people, especially Mona and Alan Wong, who constantly remind me how silly I must be to have to stay at school for **SO** long.

ABSTRACT

This work is an investigation into the physicochemical and structural properties of two tridentate, antitumour ligand systems and is divided into two sections. In the first (Chapters 1 to 4), the ligand 2-formylpyridine thiosemicarbazone (LH - containing an NNS donor set), several of its congeners and a range of complexes (predominantly Cu(II)) were prepared. The second section (Chapters 5 and 6) deals with a range of ligands based on salicylaldehyde benzoylhydrazone (sbH₂ - containing an ONO donor set), their complexes (predominantly Cu(II)) and the cytotoxicity data for all of this work.

In Chapter 1, complexes of the general formulation [CuLX]₂ for the deprotonated and [Cu(LH)X]₂X₂ for the neutral, protonated ligand were prepared (where X = e.g. halide, pseudohalide, NO₃⁻, ClO₄⁻, CH₃COO⁻, CF₃COO⁻). The complexes formed are very stable in strong, non-oxidising acid solutions and with mildly reducing anions, but are susceptible to oxidising acids and anions. The crystal structures of the neutral ligand, dimeric, one-atom anion bridged complex [Cu(LH)(CF₃COO)]₂(CF₃COO)₂ and the monomeric complex [Cu(LH)(ClO₄)₂H₂O]·2H₂O with axially coordinated perchlorato groups were determined.

In Chapter 2, the possibility that *in vivo* S and N donor atom adducts of CuL⁺ may form was investigated *in vitro*. Stable complexes containing a copper(II)-thiolato bond were isolated at ambient temperatures, under aerobic conditions. The e.s.r. parameters for these were very similar to a species formed from the interaction of CuL⁺ with human blood components. Ternary, Lewis-base adducts of nitrogen donor atoms were also isolated, and the crystal structures for two of these, [CuL(2,2'-bipyridyl)]ClO₄ and [CuL(saccharinato)H₂O]·½H₂O, were solved.

The possibility of CuL⁺ interacting with O donor groups (in particular phosphates) *in vivo* was investigated *in vitro* in Chapter 3. The ternary complexes isolated contain the anions mono-

and dihydrogenphosphate, pyrophosphate, phenolate and molybdate. The crystal structure of $[\text{Cu}(\text{LH})(\text{H}_2\text{PO}_4)]_2(\text{H}_2\text{PO}_4)_2(\text{H}_3\text{PO}_4)_2 \cdot 2\text{H}_2\text{O}$ showed the complex is dimeric, having a unique one-atom dihydrogenphosphate bridge, three inequivalent phosphates and a very strong interphosphate hydrogen-bond. In contrast, the ternary, pyrophosphato complex $[(\text{CuL})_4\text{P}_2\text{O}_7] \cdot 12\text{H}_2\text{O}$ is a tetramer, with each Cu(II) centre having a one-atom S, a three-atom pyrophosphato and two five-atom pyrophosphato bridges.

The low temperature magnetic properties of $[\text{CuL}(\text{CH}_3\text{COO})]_2$ fit the Bleaney-Bowers expression well, whereas for $[(\text{CuL})_4\text{P}_2\text{O}_7] \cdot 12\text{H}_2\text{O}$ a very weak interaction through the five-atom pyrophosphato bridge may account for the non-dimeric behaviour observed. Both complexes are weakly antiferromagnetic ($-2J \sim 6 \text{ cm}^{-1}$).

In Chapter 4, four variations on the ligand LH and a representative series of their Cu(II) complexes were synthesised. Reduction potentials for a Cu(II) complex of each ligand, as well as for two thiolato and a Lewis-base adduct of CuL^+ , were measured. N.m.r. spectroscopy was used to characterise the ligands and pKa values for both the ligands and their Cu(II) complexes were determined. No correlation between any of these values and the cytotoxicities was found.

In Chapter 5, Section 2, a range of ligands based on sbH₂ (salicylaldehyde benzoylhydrazone) and their transition metal complexes (predominantly Cu(II)) were synthesised for cytotoxicity trials (on the cell line HCT-8). A number of the Cu(II) complexes had depressed room temperature magnetic moments and displayed e.s.r. spectral features which were attributed to magnetic interactions in the solid state. The crystal structure of $[\text{Cu}(\text{sbH})\text{ClO}_4(\text{EtOH})]_2$ revealed it to be a planar, side-by-side dimer with $\text{Cu}(\text{sbH})^+$ moieties bridged via the phenolato-oxygens.

Depending upon the pH, sbH₂ can coordinate as either a neutral, monoanionic or dianionic moiety to transition metals. The interaction of $\text{CuF}_2 \cdot 2\text{H}_2\text{O}$ in HF with sbH₂ resulted in the *in*

situ formation of H_2SiF_6 . The crystal structure of the resulting complex, $[(\text{Cu}(\text{sbH})\text{H}_2\text{O})_2\text{SiF}_6]\cdot 2\text{H}_2\text{O}$, showed it to be a dimer, with the Cu(II) centres linked by the coordinated SiF_6^{2-} anion. The crystal structure of a cytotoxically inactive $\text{Cu}(\text{sbH})^+$ analogue, $[\text{Cu}(\text{saH})\text{Cl}(\text{H}_2\text{O})]\text{H}_2\text{O}$ was also solved.

In the final chapter, the cytotoxicity data for all compounds tested are presented. The copper(II) complexes generally showed activities different to the metal free ligands. For LH congeners the complexes were no better than the ligands; in contrast to the sbH_2 analogues where the Cu(II) chelates were statistically more cytotoxic. Transition metals other than Cu(II) either did not improve the activity or resulted in a reduction or loss of cytotoxicity.

For LH congeners, changes in cytotoxicity could be related to altered electronic and steric properties, whereas for the sbH_2 series of compounds, statistical analysis showed the lipophilicity conferred by a substituent to be the dominant factor. Comparisons with proven anticancer drugs are made and possible future studies to maximise the biological activity are suggested. All of the compounds tested for their antiviral activity were either cytotoxic or inactive at the concentrations used.

ACKNOWLEDGEMENTS

Much of this work would not have been possible without the gratefully acknowledged contributions from the following people:

Drs E W Ainscough and A M Brodie for their supervision and contagious enthusiasm.

Dr J M Waters for her guidance and expertise with the X-ray crystallography.

Drs W A Denny and G J Finlay, Cancer Research Laboratory, Auckland Medical School, for very generously determining the cytotoxicity data.

Dr G E Norris for solving one of the X-ray crystallographic structures and for proof reading this work.

Dr K W Jolley and Mr M H Smith for running n.m.r. spectra.

Professor R Hodges, Massey University, and Dr G J Shaw and Mr J M Allen, DSIR, Palmerston North, for running mass spectra.

Dr W T Robinson, Canterbury University, for collecting three X-ray diffraction data sets.

Dr K S Murray and Mr C Delfs, Monash University, for low temperature magnetic data.

Dr J W Blunt, Canterbury University, for kindly carrying out the antiviral assays.

Dr G A Bowmaker, Auckland University, for guidance and the use of electrochemical apparatus.

Professor A D Campbell, Otago University, for microanalytical data.

Diane Reay for typing this tome.

I would also like to sincerely thank everyone else who contributed with helpful discussions and I am also indebted to Massey University for the position of Graduate Assistant during my studies.

TABLE OF CONTENTS

	Page
Dedication	ii
Abstract	iii
Acknowledgements	vi
Contents	vii
Abbreviations	x
Index of Figures	xiii
Index of Tables	xviii
General Introduction	1
Introduction to Section 1	20
Section 1: Studies on the 2-Formylpyridine Thiosemicarbazone (LH) Ligand System	
<hr/>	
Chapter 1: Halide and Pseudohalide Copper Complexes of LH/L⁻	34
1.1.1 Introduction	34
1.1.2 Crystal Structure of [Cu(LH)(CF ₃ COO)] ₂ (CF ₃ COO) ₂ (Di-μ-trifluoroacetato-bis[(2-formylpyridine thiosemicarbazone)copper(II)] Bistrifluoroacetate)	37
1.1.3 Crystal structure of [Cu(LH)(ClO ₄) ₂ H ₂ O]·2H ₂ O (Aqua(2-formylpyridine thiosemicarbazone diperchlorato)copper(II) Dihydrate)	49
1.1.4 Results and Discussion	56
1.1.5 Experimental	72

Chapter 2:	Ternary S and N Donor Atom Copper Complexes of L⁻	88
1.2.1	Introduction	88
1.2.2	Crystal Structure of [CuL(sacc)H ₂ O]·½H ₂ O (Aqua(2-formylpyridine thiosemicarbazonato)(saccharinato-N)copper(II) Hemihydrate)	91
1.2.3	Crystal Structure of [CuL(bipy)]ClO ₄ (2, 2'-bipyridyl(2-formylpyridine thiosemicarbazonato)copper(II) Perchlorate)	100
1.2.4	Results and Discussion	108
1.2.5	Experimental	128
Chapter 3:	Ternary O Donor Atom Copper Complexes of LH/L⁻	141
1.3.1	Introduction	141
1.3.2	Crystal Structure of [(CuL) ₄ P ₂ O ₇]·12H ₂ O (μ ₄ -Pyrophosphato-tetrakis[(2-formylpyridine thiosemicarbazonato)copper(II)] Dodecahydrate)	143
1.3.3	Crystal Structure of [Cu(LH)(H ₂ PO ₄)] ₂ (H ₂ PO ₄) ₂ (H ₃ PO ₄) ₂ ·2H ₂ O (Di-μ-dihydrogenphosphato-bis[(2-formylpyridine thiosemicarbazone)copper(II) Bis(dihydrogenphosphate) Bis(trihydrogenphosphate) Dihydrate)	158
1.3.4	Results and Discussion	168
1.3.5	Experimental	183
Chapter 4:	Variations on the Cu/LH System	194
1.4.1	Introduction	194
1.4.2	Results and Discussion	195
1.4.3	Experimental	221
1.4.4	Section 1 Summary	226

Introduction to Section 2	227
Section 2: Studies on the Salicylaldehyde Benzoylhydrazone (sbH₂) System	
Chapter 5: Studies on sbH₂ Congeners and their Complexes	236
2.5.1 Introduction	236
2.5.2 Crystal Structure of [(Cu(sbH)H ₂ O) ₂ SiF ₆].2H ₂ O (μ-Hexafluorosilicato-bis[aqua(salicylaldehyde benzoylhydrazonato(1-)copper(II)] Dihydrate	240
2.5.3 Crystal Structure of Bisethanoldiperchloratobis- (μ-[salicylaldehyde benzoylhydrazonato(1-)]-μ-O, N, O')dicopper(II))	253
2.5.4 Crystal Structure of Aquachloro (salicylaldehyde acetylhydrazonato(1-))copper(II) Hydrate)	259
2.5.4 Results and Discussion	266
2.5.5 Experimental	297
Chapter 6: Cytotoxicity Results	316
2.6.1 Introduction	316
2.6.2 Results and Discussion	319
Appendix 1 General Techniques	341
Appendix 2 Reagents	343
Appendix 3 Molar Conductivities	345
Appendix 4 Miscellaneous Reactions for Section 1	346
References	348

ABBREVIATIONS

a.a.	atomic absorption
a.m.u.	atomic mass units
bipy ^a	2, 2'-bipyridyl
cisplatin ^b	<i>cis</i> -diamminedichloroplatinum(II)
c.t.	charge transfer
dips	diisopropylsalicylic acid
dmap	4-N,N-dimethylaminopyridine
dmf	dimethylformamide
dmso	dimethylsulphoxide
DNA	deoxyribonucleic acid
edta	ethylenediaminetetraacetic acid
en	ethylenediamine
e.s.d.	estimated standard deviation
e.s.r.	electron spin resonance
H	in a ligand or complex refers to an ionisable proton
Hb	haemoglobin
IC ₅₀	inhibitory concentration to 50%; the concentration required to inhibit cell growth to 50% compared with that of a control
ir	infrared
LD ₅₀	lethal dose to 50%; the single injected dose that kills 50% of the animals
LH ^{a,c}	2-formylpyridine thiosemicarbazone
2'L ^c	2-formylpyridine 2'-methylthiosemicarbazone
4'LH ^c	2-formylpyridine 4'-methylthiosemicarbazone
6LH ^c	6-methyl-2-formylpyridine thiosemicarbazone
mbtH ^a	2-mercaptobenzothiazole
miH ^a	2-mercaptoimidazole
mmiH ^a	2-mercapto-1-methylimidazole

mpH ₂ ^a	2-mercapto-3-pyridinol
m.t.	mull transmittance
mttH ^a	4-methyl-1,2,4-triazole-3-thiol
n.m.r.	nuclear magnetic resonance
ntpH	4-nitrothiophenol
pbH ^a	2-formylpyridine benzoylhydrazone
pctpH	pentachlorothiophenol
pftpH	pentafluorothiophenol
phen ^a	1,10-phenanthroline
ptpH ^a	paratrylphenol
py	pyridine
rdr ^e	ribonucleoside diphosphate reductase (ribonucleotide reductase)
RNA	ribonucleic acid
saH ₂ ^{a,d}	salicylaldehyde acetylhydrazone
sbH ₂ ^{a,d}	salicylaldehyde benzoylhydrazone
spy	square-pyramidal
tipH	2,4,6-triiodophenol
tby	trigonal-bipyramidal
TMS	tetramethylsilane
uv/vis	ultraviolet/visible

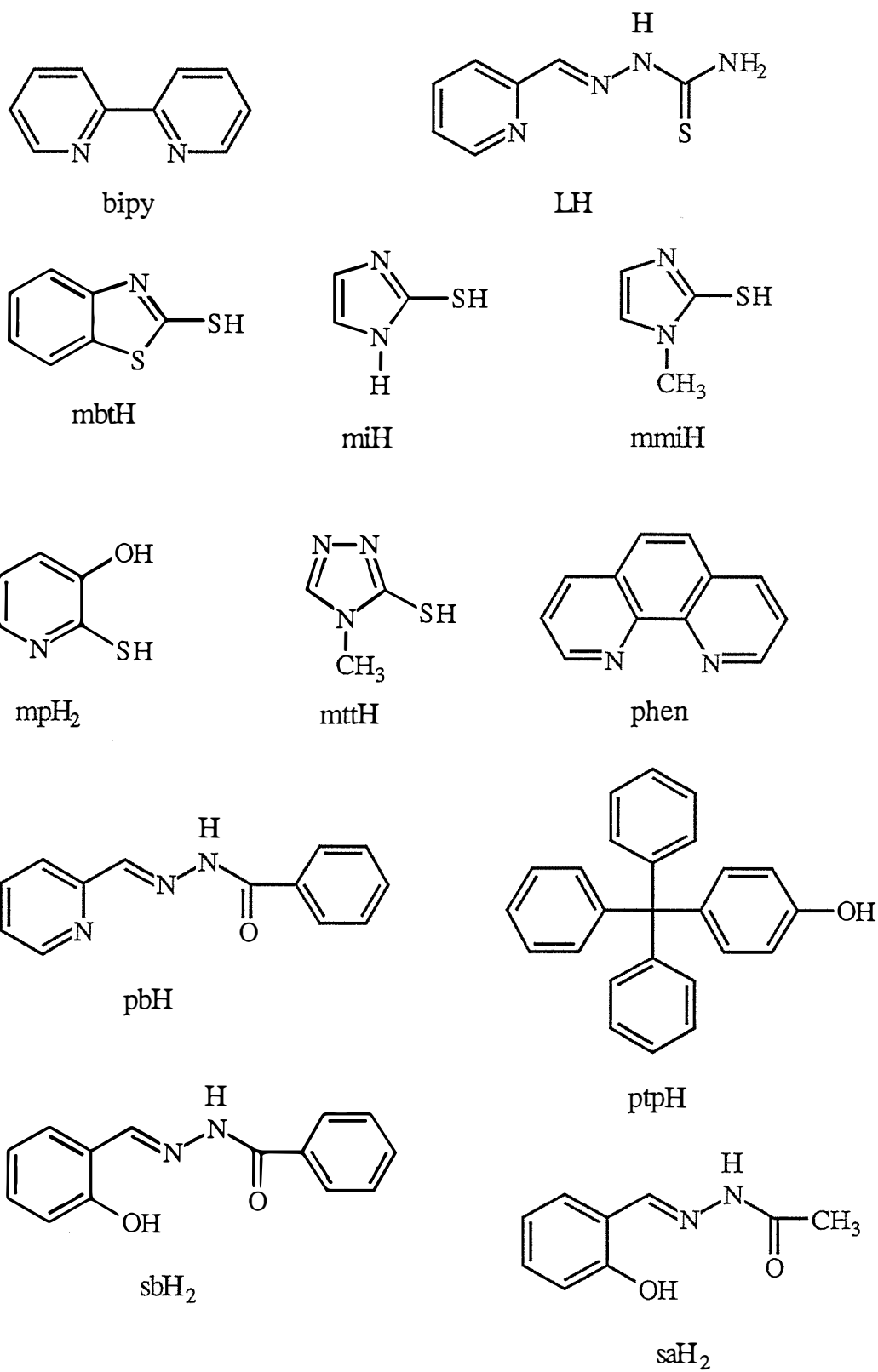
a structure abbreviated on following page

b see Figure 1.1

c see Figure 4.1 in Chapter 4 introduction

d see Figure 2.5.11 for this and all other structurally related ligands for Section 2

e see Figure 1.4



Figures for the abbreviations.

INDEX OF FIGURES

	Page
 General Introduction	
Figure 1.1 The structures of some platinum anticancer drugs	3
Figure 1.2 Profile of copper levels at onset of neoplasia through therapy induced or spontaneous remission	8
Figure 1.3 Examples of three ligands which require copper for biological activity	9
Figure 1.4 Schematic diagram of ribonucleoside diphosphate reductase (rdr)	12
Figure 1.5 The two basic ligand systems used in this study	15
Figure 1.6 Some structural examples of tridentate ligands	16
 Section 1	
 Introduction to Section 1	
Figure 1.7 Conformations of thiosemicarbazide: bidentate (<i>cis</i>) and monodentate (<i>trans</i>)	21
Figure 1.8 Reaction scheme for the formation of thiosemicarbazones	22
Figure 1.9 Coordination modes of bidentate thiosemicarbazones	23
Figure 1.10 An example of a tridentate thiosemicarbazone: 2-formylpyridine thiosemicarbazone (LH)	23
Figure 1.11 An example of a tetradentate thiosemicarbazone	24
Figure 1.12 Resonance forms for 2-formylpyridine thiosemicarbazone	28
Figure 1.13 Schematic diagrams for the coordination modes of NNS tridentate thiosemicarbazones	29

Chapter 1

- Figure 1.1.1** The dimeric cation for $[\text{Cu}(\text{LH})(\text{CF}_3\text{COO})]_2(\text{CF}_3\text{COO})_2$ and a non-coordinated CF_3COO^- anion (arbitrary positioning) showing the atom numbering scheme 38
- Figure 1.1.2** Stereo-view of the unit-cell packing diagram for $[\text{Cu}(\text{LH})(\text{CF}_3\text{COO})]_2(\text{CF}_3\text{COO})_2$ showing the hydrogen-bonding scheme 47
- Figure 1.1.3** The monomer $[\text{Cu}(\text{LH})(\text{ClO}_4)_2\text{H}_2\text{O}] \cdot 2\text{H}_2\text{O}$ showing the atom numbering scheme 50
- Figure 1.1.4** Stereo-view of the unit-cell packing diagram for $[\text{Cu}(\text{LH})(\text{ClO}_4)_2\text{H}_2\text{O}] \cdot 2\text{H}_2\text{O}$ 54
- Figure 1.1.5** Powder e.s.r. spectra for $[\text{Cu}(\text{LH})(\text{ClO}_4)_2\text{H}_2\text{O}] \cdot 2\text{H}_2\text{O}$ at 110 K showing the $g = 2$ ($\Delta M_s = 1$) and $g = 4$ ($\Delta M_s = 2$) regions 68

Chapter 2

- Figure 1.2.1** The monomer $[\text{CuL}(\text{sacc})\text{H}_2\text{O}] \cdot \frac{1}{2}\text{H}_2\text{O}$ showing the atom numbering scheme 92
- Figure 1.2.2** Stereo-view of the unit-cell packing diagram for $[\text{CuL}(\text{sacc})\text{H}_2\text{O}] \cdot \frac{1}{2}\text{H}_2\text{O}$ showing the hydrogen-bonding scheme 98
- Figure 1.2.3** The monomeric cation for $[\text{CuL}(\text{bipy})]\text{ClO}_4$ showing the atom numbering scheme 101
- Figure 1.2.4** The copper coordination environment for $[\text{CuL}(\text{bipy})]\text{ClO}_4$ viewed from (a) trigonal-bipyramidal and (b) square-pyramidal geometries 103
- Figure 1.2.5** Stereo-view of the unit-cell packing diagram for $[\text{CuL}(\text{bipy})]\text{ClO}_4$ 106
- Figure 1.2.6** Plot of $10^4 |A_{\parallel}|$ (cm^{-1}) vs. g_{\parallel} for various in-plane donor atom sets 113
- Figure 1.2.7** Some typical e.s.r. spectra at 110 K
 (a) $[\text{CuL}(\text{CH}_3\text{COO})]_2$ in 90% EtOH/10% dmsO
 (b) $[\text{CuL}(\text{pctp})]_2$ in 90% EtOH/10% dmsO
 (c) $[\text{CuL}(\text{pctp})]_2$ powder
 (d) $[\text{CuL}(\text{bipy})]\text{ClO}_4$ powder 115
- Figure 1.2.8** E.s.r. spectrum for $[\text{Cu}(\text{mpH})_2]$ in dmsO at 110 K 117
- Figure 1.2.9** E.s.r. spectrum for $[\text{CuL}(\text{CH}_3\text{COO})]_2$ in human red cells with 5% dmsO at 110 K 121

Chapter 3

- Figure 1.3.1** The tetramer $[(\text{CuL})_4\text{P}_2\text{O}_7]\cdot 12\text{H}_2\text{O}$ showing the atom numbering scheme 144
- Figure 1.3.2** The tetramer $[(\text{CuL})_4\text{P}_2\text{O}_7]\cdot 12\text{H}_2\text{O}$ showing the long, apical Cu-S bonds 145
- Figure 1.3.3** The $\text{P}_2\text{O}_7^{4-}$ moiety for $[(\text{CuL})_4\text{P}_2\text{O}_7]\cdot 12\text{H}_2\text{O}$ showing the staggered arrangement 152
- Figure 1.3.4** Unit-cell packing diagram for $[(\text{CuL})_4\text{P}_2\text{O}_7]\cdot 12\text{H}_2\text{O}$ 152
- Figure 1.3.5** View of two $[(\text{CuL})_4\text{P}_2\text{O}_7]\cdot 12\text{H}_2\text{O}$ tetramers with selected water molecules and hydrogen-bonds 156
- Figure 1.3.6** View showing the stacking for $[(\text{CuL})_4\text{P}_2\text{O}_7]\cdot 12\text{H}_2\text{O}$ tetramers with the same hydrogen-bonds as Figure 1.3.5 156
- Figure 1.3.7** View of symmetry related CuL^+ moieties for $[(\text{CuL})_4\text{P}_2\text{O}_7]\cdot 12\text{H}_2\text{O}$ showing the stacking and partial pyridine ring overlap 157
- Figure 1.3.8** The dimeric cation for $[\text{Cu}(\text{LH})(\text{H}_2\text{PO}_4)]_2(\text{H}_2\text{PO}_4)_2(\text{H}_3\text{PO}_4)_2\cdot 2\text{H}_2\text{O}$ showing the atom numbering scheme 159
- Figure 1.3.9** Stereo-view of the unit-cell packing diagram for $[\text{Cu}(\text{LH})(\text{H}_2\text{PO}_4)]_2(\text{H}_2\text{PO}_4)_2(\text{H}_3\text{PO}_4)_2\cdot 2\text{H}_2\text{O}$ 166
- Figure 1.3.10** The hydrogen-bonding schemes around each of the three phosphate species for $[\text{Cu}(\text{LH})(\text{H}_2\text{PO}_4)]_2(\text{H}_2\text{PO}_4)_2(\text{H}_3\text{PO}_4)_2\cdot 2\text{H}_2\text{O}$
 (a) the coordinated bridging H_2PO_4^- anion
 (b) the non-coordinated ' H_2PO_4^- '
 (c) the non-coordinated ' H_3PO_4 ' molecule 167
- Figure 1.3.11** Temperature dependence of $[\text{CuL}(\text{CH}_3\text{COO})]_2$ for
 (a) the molecular susceptibilities, and
 (b) the magnetic moments 173
- Figure 1.3.12** Temperature dependence of $[(\text{CuL})_4\text{P}_2\text{O}_7]\cdot 12\text{H}_2\text{O}$ for
 (a) the molecular susceptibilities, and
 (b) the magnetic moments 174

Chapter 4

- Figure 4.1** Ligands used in this chapter 194
- Figure 1.4.1** Spectral forms for $\text{Cu}(\text{4L})^+$ as a function of pH 204
- Figure 1.4.2** ^1H - ^1H shift correlation (cosy) spectrum for LH 211

Figure 1.4.3	^1H - ^{13}C shift correlation (hetcor) spectrum for LH	212
Figure 1.4.4	J-resolved spectrum for LH with the decoupled ^1H spectrum	213
Figure 1.4.5	Slices through the J-resolved peaks for LH	214

Section 2

Introduction to Section 2

Figure 2.1	The structures of selected compounds related to salicylic acid	228
Figure 2.2	The structures of (a) salicylaldehyde benzoylhydrazone (sbH ₂) and (b) 2-formylpyridine-2'-pyridylhydrazone (papH)	231

Chapter 5

Figure 2.5.1	The dimer [(Cu(sbH)H ₂ O) ₂ SiF ₆] \cdot 2H ₂ O showing the atom numbering scheme	241
Figure 2.5.2	Some canonical forms of salicylaldehyde benzoylhydrazone (sbH ₂)	247
Figure 2.5.3	The dimer [(Cu(sbH)H ₂ O) ₂ SiF ₆] \cdot 2H ₂ O showing the atom numbering scheme and the hydrogen-bonding scheme	248
Figure 2.5.4	(a) side-view of three [(Cu(sbH)H ₂ O) ₂ SiF ₆] \cdot 2H ₂ O molecules (b) plan-view of the top two stacked molecules from (a) (c) plan-view of the bottom two stacked molecules from (a) (d) stereo-view of the unit-cell packing diagram	249
Figure 2.5.5	The dimer [Cu(sbH)ClO ₄ (EtOH)] ₂ showing the atom numbering scheme	254
Figure 2.5.6	The dimer [Cu(sbH)ClO ₄ (EtOH)] ₂ showing the atom numbering scheme and planar side-by-side structure	255
Figure 2.5.7	Cut-away view of the dimer [Cu(sbH)ClO ₄ (EtOH)] ₂ showing the hydrogen-bonding scheme	255
Figure 2.5.8	Stereo-view of the unit-cell packing diagram for [Cu(sbH)ClO ₄ (EtOH)] ₂	257
Figure 2.5.9	The monomer [Cu(saH)Cl(H ₂ O)]H ₂ O showing the atom numbering scheme	260
Figure 2.5.10	Stereo-view of the unit-cell packing diagram for [Cu(saH)Cl(H ₂ O)]H ₂ O showing the hydrogen-bonding	264

scheme

- Figure 2.5.11** Abbreviations used for ligands in chapters 5 and 6 268
- Figure 2.5.12** Schematic diagrams for the structures of 278
 (a) acetylacetonone-mono(*o*-hydroxyanil)copper(II)
 (b) copper(II) carboxylates
 (c) (pyridine *N*-oxide)copper(II) chloride
- Figure 2.5.13** Powder e.s.r. spectra for [Cu(*sbH*)ClO₄(H₂O)]₂ at 110 K 283
 (a) $g = 2$ ($\Delta M_s = 1$) and (b) $g = 4$ ($\Delta M_s = 2$) regions
- Figure 2.5.14** ¹H–¹³C shift correlation (hetcor) spectrum for *sbH*₂ 288
- Figure 2.5.15** (a) J-resolved spectrum for *sbH*₂ with the decoupled ¹H spectrum, and (b) slices through the J-resolved peaks for *sbH*₂ 289
- Figure 2.5.16** Possible conformers for hydrazones 293
- Figure 2.5.17** (a) ¹H–¹³C shift correlation (hetcor) spectrum and 294
 (b) ¹H–¹H shift correlation (cosy) spectrum for *saH*₂
- Figure 2.5.18** The two *E*-form conformers for *saH*₂ 295
- Chapter 6**
- Figure 2.6.1** The monomeric cation for [Cu(6L)(bipy)]Cl showing 322
 selected atom numbering and the difference in selected bond angles and distances between this structure and [CuL(bipy)]ClO₄
- Figure 2.6.2** Plot of log 1/(IC₅₀) vs. lipophilicity for *sbH*₂ congeners 332
 substituted into the benzoyl ring and their corresponding copper(II) complexes
- Figure 2.6.3** Plot of log 1/(IC₅₀) vs. lipophilicity for all *sbH*₂ congeners 333
 and their corresponding copper(II) complexes

INDEX OF TABLES

		Page
General Introduction		
Table 1.1	Recognized copper-dependent enzymes and their biochemical function	7
 Section 1		
 Introduction to Section 1		
Table 1.2	Some examples of thiosemicarbazones	26
 Chapter 1		
Table 1.1.1	Analytical and magnetic data for chapter 1	36
Table 1.1.2	Bond lengths (Å) with estimated standard deviations in parentheses for the complexes $[\text{Cu}(\text{LH})(\text{ClO}_4)_2\text{H}_2\text{O}] \cdot 2\text{H}_2\text{O}$	39
Table 1.1.3	Bond angles (°) with estimated standard deviations in parentheses for the complexes $[\text{Cu}(\text{LH})(\text{ClO}_4)_2\text{H}_2\text{O}] \cdot 2\text{H}_2\text{O}$ and $[\text{Cu}(\text{LH})(\text{CF}_3\text{COO})]_2(\text{CF}_3\text{COO})_2$	40
Table 1.1.4	Bond distances (Å) for in-plane coordinating atoms of Cu and LH/L ⁻	42
Table 1.1.5	Comparison of thiosemicarbazone bond lengths (Å)	42
Table 1.1.6	Bond lengths (Å) and angles (°) about C(7) in thiosemicarbazide and thiosemicarbazone compounds	44
Table 1.1.7	Hydrogen-bonding distances (Å) and angles (°) for $[\text{Cu}(\text{LH})(\text{CF}_3\text{COO})]_2(\text{CF}_3\text{COO})_2$	46
Table 1.1.8	Selected data for some copper(II) diperchlorato complexes	53
Table 1.1.9	Hydrogen-bonding distances (Å) and angles (°) for $[\text{Cu}(\text{LH})(\text{ClO}_4)_2\text{H}_2\text{O}] \cdot 2\text{H}_2\text{O}$	55
Table 1.1.10	Absorption maxima and conductance data for chapter 1	57
Table 1.1.11	Selected ir spectral bands (cm ⁻¹) for representative chapter 1 compounds	63

Table 1.1.12	Anion infrared bands for chapter 1	64
Table 1.1.13	E.s.r. results for selected chapter 1 complexes	67
Table 1.1.14	Crystal data for $[\text{Cu}(\text{LH})(\text{CF}_3\text{COO})]_2(\text{CF}_3\text{COO})_2$	82
Table 1.1.15	Parameters associated with data collection for $[\text{Cu}(\text{LH})(\text{CF}_3\text{COO})]_2(\text{CF}_3\text{COO})_2$	83
Table 1.1.16	Crystal data for $[\text{Cu}(\text{LH})(\text{ClO}_4)_2\text{H}_2\text{O}] \cdot 2\text{H}_2\text{O}$	86
Table 1.1.17	Parameters associated with data collection for $[\text{Cu}(\text{LH})(\text{ClO}_4)_2\text{H}_2\text{O}] \cdot 2\text{H}_2\text{O}$	87

Chapter 2

Table 1.2.1	Analytical and magnetic data for chapter 2	90
Table 1.2.2	Bond lengths (Å) with estimated standard deviations in parentheses for the complexes $[\text{CuL}(\text{sacc})\text{H}_2\text{O}] \cdot \frac{1}{2}\text{H}_2\text{O}$ and $[\text{CuL}(\text{bipy})]\text{ClO}_4$	93
Table 1.2.3	Bond angles (°) with estimated standard deviations in parentheses for the complexes $[\text{CuL}(\text{sacc})\text{H}_2\text{O}] \cdot \frac{1}{2}\text{H}_2\text{O}$ and $[\text{CuL}(\text{bipy})]\text{ClO}_4$	94
Table 1.2.4	Selected bond lengths (Å) and angles (°) for saccharin compounds	97
Table 1.2.5	Hydrogen-bonding distances (Å) and angles (°) for $[\text{CuL}(\text{sacc})\text{H}_2\text{O}] \cdot \frac{1}{2}\text{H}_2\text{O}$	99
Table 1.2.6	Hydrogen-bonding distances (Å) and angles (°) for $[\text{CuL}(\text{bipy})]\text{ClO}_4$	103
Table 1.2.7	Absorption maxima and conductance data for chapter 2	109
Table 1.2.8	E.s.r. results for selected chapter 2 complexes	112
Table 1.2.9	E.s.r. results for CuL^+ with human blood components	120
Table 1.2.10	Crystal data for $[\text{CuL}(\text{sacc})\text{H}_2\text{O}] \cdot \frac{1}{2}\text{H}_2\text{O}$	135
Table 1.2.11	Parameters associated with data collection for $[\text{CuL}(\text{sacc})\text{H}_2\text{O}] \cdot \frac{1}{2}\text{H}_2\text{O}$	136
Table 1.2.12	Crystal data for $[\text{CuL}(\text{bipy})]\text{ClO}_4$	139
Table 1.2.13	Parameters associated with data collection for $[\text{CuL}(\text{bipy})]\text{ClO}_4$	140

Chapter 3

Table 1.3.1	Analytical and magnetic data for chapter 3	142
Table 1.3.2	Bond lengths (Å) with estimated standard deviations in parentheses for the complex [(CuL) ₄ P ₂ O ₇].12H ₂ O	146
Table 1.3.3	Bond angles (°) with estimated standard deviations in parentheses for the complex [(CuL) ₄ P ₂ O ₇].12H ₂ O	147
Table 1.3.4	Hydrogen-bonding distances (Å) for [(CuL) ₄ P ₂ O ₇].12H ₂ O	154
Table 1.3.5	Bond lengths (Å) with estimated standard deviations in parentheses for the complex [Cu(LH)(H ₂ PO ₄) ₂](H ₂ PO ₄) ₂ (H ₃ PO ₄) ₂ .2H ₂ O	160
Table 1.3.6	Bond angles (°) with estimated standard deviations in parentheses for the complex [Cu(LH)(H ₂ PO ₄) ₂](H ₂ PO ₄) ₂ (H ₃ PO ₄) ₂ .2H ₂ O	160
Table 1.3.7	Selected bond distance (Å) and angle (°) data for centrosymmetric anion bridged complexes of copper(II) with LH/L ⁻	162
Table 1.3.8	Hydrogen-bonding distances (Å) and angles (°) for [Cu(LH)(H ₂ PO ₄) ₂](H ₂ PO ₄) ₂ (H ₃ PO ₄) ₂ .2H ₂ O	162
Table 1.3.9	Absorption maxima and conductance data for chapter 3	169
Table 1.3.10	Selected anion infrared bands for chapter 3	171
Table 1.3.11	Theoretical values of 2J from μ _{eff} and g _i	171
Table 1.3.12	Selected e.s.r. results for chapter 3 complexes	178
Table 1.3.13	Crystal data for [(CuL) ₄ P ₂ O ₇].12H ₂ O	188
Table 1.3.14	Parameters associated with data collection for [(CuL) ₄ P ₂ O ₇].12H ₂ O	189
Table 1.3.15	Crystal data for [Cu(LH)(H ₂ PO ₄) ₂](H ₂ PO ₄) ₂ (H ₃ PO ₄) ₂ .2H ₂ O	192
Table 1.3.16	Parameters associated with data collection for [Cu(LH)(H ₂ PO ₄) ₂](H ₂ PO ₄) ₂ (H ₃ PO ₄) ₂ .2H ₂ O	193

Chapter 4

Table 1.4.1	Analytical and magnetic data for chapter 4	196
Table 1.4.2	Absorption maxima and conductance data for chapter 4	198
Table 1.4.3	Selected e.s.r. results for chapter 4 complexes	201

Table 1.4.4	E.s.r. results for $\text{Cu}(2'L)^{2+}$ and $\text{Cu}(\text{pb})^+$ with human blood components	201
Table 1.4.5	Protonation constants and reduction potentials for selected section 1 compounds	205
Table 1.4.6	Selected nuclear magnetic resonance data for LH type compounds	215
Table 1.4.7	^1H n.m.r. data for LH type compounds	216

Section 2

Chapter 5

Table 2.5.1	Analytical and physical data for chapter 5 ligands	238
Table 2.5.2	Analytical and magnetic data for chapter 5 complexes	239
Table 2.5.3	Bond lengths (\AA) with estimated standard deviations in parentheses for the complexes $[(\text{Cu}(\text{sbH})\text{H}_2\text{O})_2\text{SiF}_6]\cdot 2\text{H}_2\text{O}$ and $[\text{Cu}(\text{sbH})\text{ClO}_4(\text{EtOH})]_2$	242
Table 2.5.4	Bond angles ($^\circ$) with estimated standard deviations in parentheses for the complexes $[(\text{Cu}(\text{sbH})\text{H}_2\text{O})_2\text{SiF}_6]\cdot 2\text{H}_2\text{O}$ and $[\text{Cu}(\text{sbH})\text{ClO}_4(\text{EtOH})]_2$	243
Table 2.5.5	Copper bond lengths in $\text{Cu}(\text{sbH})^+$ and some related complexes	245
Table 2.5.6	Comparison of salicylaldehyde benzoylhydrazonato and salicylaldehyde acetylhydrazonato bond lengths (\AA)	245
Table 2.5.7	Hydrogen-bonding distances (\AA) and angles ($^\circ$) for $[(\text{Cu}(\text{sbH})\text{H}_2\text{O})_2\text{SiF}_6]\cdot 2\text{H}_2\text{O}$	250
Table 2.5.8	Bond lengths (\AA) with estimated standard deviations in parentheses for the complex $[\text{Cu}(\text{saH})\text{Cl}(\text{H}_2\text{O})]\text{H}_2\text{O}$	261
Table 2.5.9	Bond angles ($^\circ$) with estimated standard deviations in parentheses for the complex $[\text{Cu}(\text{saH})\text{Cl}(\text{H}_2\text{O})]\text{H}_2\text{O}$	261
Table 2.5.10	Hydrogen-bonding distances (\AA) and angles ($^\circ$) for $[\text{Cu}(\text{saH})\text{Cl}(\text{H}_2\text{O})]\text{H}_2\text{O}$	265
Table 2.5.11	Absorption maxima and conductance data for chapter 5	269
Table 2.5.12	Selected infrared absorption bands for chapter 5	275
Table 2.5.13	Selected e.s.r. results for chapter 5 complexes	279
Table 2.5.14	^{13}C n.m.r. data for chapter 5	290

Table 2.5.15	Selected ^1H n.m.r. data for chapter 5	292
Table 2.5.16	Crystal data for $[(\text{Cu}(\text{sbH})\text{H}_2\text{O})_2\text{SiF}_6]\cdot 2\text{H}_2\text{O}$	306
Table 2.5.17	Parameters associated with data collection for $[(\text{Cu}(\text{sbH})\text{H}_2\text{O})_2\text{SiF}_6]\cdot 2\text{H}_2\text{O}$	307
Table 2.5.18	Crystal data for $[\text{Cu}(\text{sbH})\text{ClO}_4(\text{EtOH})]_2$	310
Table 2.5.19	Parameters associated with data collection for $[\text{Cu}(\text{sbH})\text{ClO}_4(\text{EtOH})]_2$	311
Table 2.5.20	Crystal data for $[\text{Cu}(\text{saH})\text{Cl}(\text{H}_2\text{O})]\text{H}_2\text{O}$	314
Table 2.5.21	Parameters associated with data collection for $[\text{Cu}(\text{saH})\text{Cl}(\text{H}_2\text{O})]\text{H}_2\text{O}$	315
 Chapter 6		
Table 2.6.1	Cytotoxicity data for section 1 compounds	320
Table 2.6.2	Cytotoxicity data for section 2 compounds	329